ELSEVIER

Materials Characterization 54 (2005) 315–326

MATERIALS CHARACTERIZATION

Optical anisotropy of a color-etched AZ91 magnesium alloy

A. Maltais, D. Dubé*, F. Roy, M. Fiset

Department of Mining, Metallurgical and Materials Engineering, Pavillon Adrien-Pouliot, Université Laval, Québec, QC, Canada G1K 7P4

Received 14 October 2004; accepted 3 December 2004

Abstract

In this paper, the optical anisotropy of a color-etched AZ91 magnesium alloy grain is studied. In the first part, the rinsing and drying conditions after etching were varied in order to improve the contrast between grains. A rinsing solution was selected and ellipsometric measurements were carried out to characterize the optical anisotropy of the etched surface. The wavelength, grain orientation and angle of incidence were varied. It was found that the reflection intensity at oblique incidence and the phase shift between parallel and perpendicular polarizations depend on the orientation of the etched surface of the grains. The optical contrast under diffuse light is explained by the morphology of the surface film deposited upon etching. The optical contrast under polarized light is attributed to form birefringence induced by the film texture. The birefringence, the fast axis, the slow axis, and the optical axis of the etched surface were also determined with the polarizing microscope.

Keywords: Color etching; Magnesium–aluminum alloys; Anisotropy; Microstructure; Birefringence

1. Introduction

In a recent paper, a simple and very practical color etching method was presented for the examination of the microstructure of cast AZ91 magnesium alloy [1]. Interest in this method was revealed by studies about vibration-induced nucleation of magnesium–aluminum alloys [2,3]. This etching produces a crackled film at the surface of several Mg–Al based alloys that permits a rapid and simultaneous evaluation of grain size, grain texture and dendrite arms spacing [4]. The etched grains are readily visible under diffuse light and under cross-polarized light.

The main advantage of this etchant is that, unlike others [5–16], it does not require a solid solution heat treatment prior to etching in order to enhance grain boundaries delineation. Such a heat treatment not only modifies the as-cast structure of Mg–Al alloys, it sometimes promotes grain growth, leading to erroneous grain size estimates [17]. It can also induce recrystallisation if the specimen has been mechanically polished prior to heating. As shown in Table 1, several heat treatments with widely varying parameters were used to accentuate grain boundaries in Mg–Al alloys.

* Corresponding author. Tel.: +1 418 656 2131x8101; fax: +1 418 656 5343.
E-mail address: ddube@gmn.ulaval.ca (D. Dubé).

1044-5803/$ - see front matter © 2005 Elsevier Inc. All rights reserved.
doi:10.1016/j.matchar.2004.04.011

Table 1
Solid solution heat treatments used to enhance grain boundaries delineation in Mg–Al alloys

Alloy	Heat treatment		Ref.
	Duration (Hour)	Temperature (°C)	
AZ91	8	400	[5]
	16–24	415	[6]
	24	400	[7]
	8–16–2	380–420–200	[8]
	6–2–10	413–352–413	[9]
AZ92	16	400–415	[10]
Mg–9%Al	2	380	[11]
	2	420	[12]
	7.2	392	[13]
Mg–(0–9%)Al	0.5	413	[14]
Mg–(0–33%)Al	2	413	[15]
Mg–3%Al, Mg–6%Al, AZ91	8–16	420–200	[16]

Although the microstructure of the crackled film responsible for color contrast under polarized light was studied and its chemical composition determined, its optical properties were not completely established [1]. Based on the disappearance of the polarization phenomena for etched specimens immersed in alcohol [18], it was concluded that the surface film exhibits "form birefringence" [1]. The present work has been carried out in order to assess the optical anisotropy of color-etched AZ91D alloy providing further evidence about the phenomena underlying the contrast between grains. Repeated observations in our laboratory have shown that the rinsing and drying conditions strongly influence the crackling pattern of the surface film, which in turn have a dramatic effect on the optical contrast between grains. Consequently, in the first part of this work, the rinsing and drying conditions were varied and their influence on the texture of the anisotropic surface film was examined.

A particular rinsing and drying procedure was selected and ellipsometric measurements were performed on a single grain of a polished specimen of AZ91D alloy to study its optical anisotropy after polishing and after line etching. In a first series of measurements, the anisotropy of reflection of unpolarized light at oblique incidence was characterized. In a second series of measurements, the birefringence of the surface at near normal incidence was determined. In both cases, the angular orientation of the textured surface, the wavelength of the incident light and the angle of incidence were varied. Further measurements were performed with a polarizing microscope in order to determine the fast axis, the slow axis and the sign of birefringence of the etched surface.

2. Theoretical background

A wide variety of color etchants, based on surface film deposition, were developed for single and multiphase alloys [19]. Generally, the color contrast is induced by variations in film thickness, as shown in Fig. 1a [20]. In this case, light is reflected at the surface film and at the film/substrate interface causing interference. Polarized light is not necessary to obtain a contrast between grains, but coloration can be intensified by using cross-, or nearly cross-, polarized light [20].

An optically anisotropic epitaxial layer, but of uniform thickness, can also create a contrast between adjacent grains due to birefringence (Fig. 1b). In this case, the incoming light splits into two beams travelling in the layer at different velocities. They recombine phase shifted when exiting the anisotropic layer producing interference. The interference intensity varies between zero and a maximum value according to the crystallographic orientation of the surface layer. Thus, if the orientation of the granular substrate and the film are related, optical contrast between grains occurs under cross-polarized light.

Surface anisotropy can also be induced by etch pitting, which leaves a characteristic surface texture as shown in Fig. 1c [21]. Upon pitting, two sets of parallel faces are formed. These faces generally follow the planes of low indices such as (100), (110) or (111) for alloys having a cubic structure [18]. Therefore, the orientation of these faces changes from one grain to the next and their crystallographic orientation can be determined by studying the anisotropy of reflection at oblique incidence with a goniometer (beam A and D in Fig. 1c) [22]. The normal incident light is elliptically polarized after being obliquely reflected twice and reflected back (beam C in Fig. 1c) or lost (beam B in Fig. 1c) [21]. Thus, the light optical microscope can be used to distinguish grains under cross-polarized light.

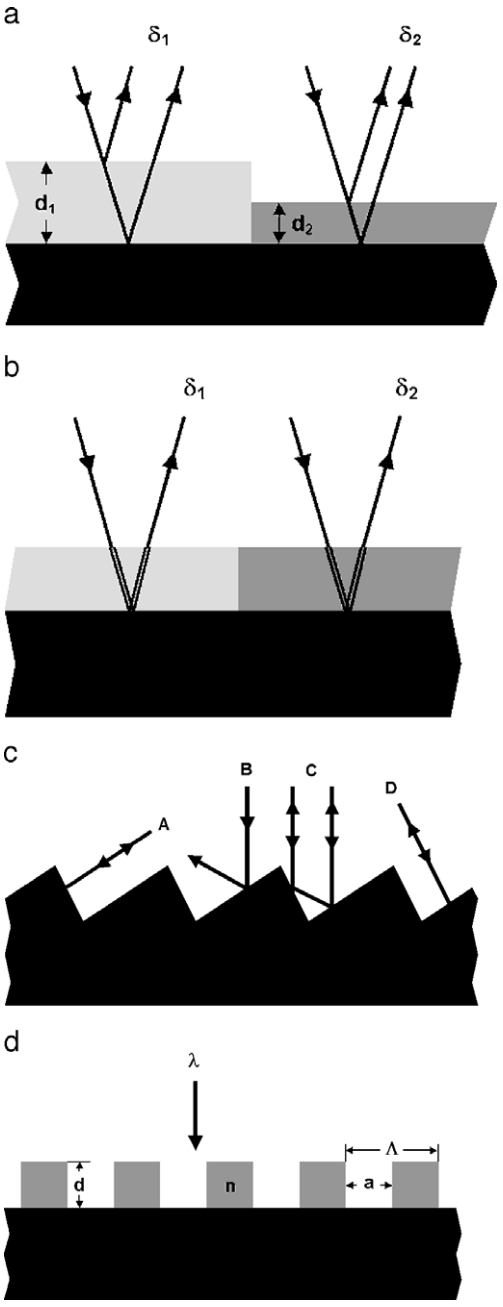

Fig. 1. Schematic cross section of optically anisotropic surfaces. (a) Interference film deposition: the variation in thickness causes a variation of interference. (b) Anisotropic film deposition: the varying orientation of the naturally anisotropic film causes a varying interference. (c) Etch pitting: the surface morphology causes polarization at normal incidence and anisotropic reflection at oblique incidence. (d) Line etching: the varying orientation of the cracks produces a variation of interference.

Line etching is another metallographic technique used to distinguish adjacent grains. In this case, a film is formed over the polished surface and crackles upon drying due to shrinking stresses. This leaves a surface with cracks preferentially aligned in one direction as shown in Fig. 1d [1]. As George [23] noted, it is possible to observe this cracking under the light optical microscope by leaving the specimen wet with alcohol and letting it dry in place on the microscope stage. The orientation of cracking changes from one grain to the next suggesting an epitaxial growth of the layer. The pattern of the crackled surface can also change with the composition of the substrate [1,23]. Thus, the grains and phases can be identified by studying the film morphology. However, if a surface grating is thick (d) enough [24] and its periodic structure size (Λ) is small enough compared to the incident wavelength (λ) [25], birefringence occurs. This birefringence depends on the refraction index (n) of the film and the fill factor ($F=1-a/\Lambda$) [25]. Thus, the polarizing microscope can be used in this case to distinguish grains and characterize their size and texture [26].

3. Materials and methods

3.1. Film texture analysis

A commercially-pure gravity-cast AZ91D magnesium alloy was selected for the analysis of film texture. A specimen of about 10 mm×10 mm and 5 mm thick was cut out from the cast part and solution heat treated at 413 °C for 24 h in order to reduce the microsegregation of the as-cast structure. As mentioned earlier, the homogenization treatment is not required to create a contrast between adjacent grains upon etching. However, the study of the film morphology is facilitated by a more uniform composition.

The AZ91D specimen was mechanically grounded and polished in accordance with the usual practice developed for magnesium alloys [27]. It was etched for 240 s in a solution containing 50 ml of distilled water, 150 ml of anhydrous ethyl alcohol and 1 ml of glacial acetic acid and then rinsed [1]. Three rinsing solutions were tested in order to modify the drying rate of the surface film and evaluate its effect on the surface texture (Table 2). After rinsing, the specimen

Table 2
Characteristics of the rinsing solutions

Rinsing solution	Reaction with AZ91	Drying rate
Anhydrous ethyl alcohol	No	High
90% Ethyl alcohol 10% Ethylene glycol	No	Very low
Distilled water	Yes	Low

was dried in a blast of air. The polishing and etching steps were repeated on the same specimen for each rinsing solution.

Indentations were practiced on the etched surface in order to take photomicrographs of exactly the same grains after rinsing in each of the three solutions (consequently light polishing was needed between each etching–rinsing–drying test). The specimen was coated with Au–Pd prior to examination with the scanning electron microscope (SEM). The acceleration voltage and the working distance were set to 15 kV and 20–21 mm, respectively.

3.2. Anisotropy analysis

Several specimens 20 mm×20 mm and 5 mm thick were cut out from the surface of a commercially pure AZ91D ingot having grains of about 10–15 mm in diameter. These specimens were also solution heat treated at 413 °C for 24 h in order to lessen the microsegregation caused by the slow solidification of the ingot. The reflected optical signal was more intense and more reproducible after homogenization of the alloy, facilitating ellipsometric measurements.

The metallographic preparation of specimens was similar to the above-described procedure used for film texture analysis. Anhydrous ethyl alcohol was selected as rinsing solution because it produces thin parallel stripes following the crystallographic orientation of the underlying grains [1]. Prior to ellipsometric measurements, polished specimens were examined with light optical microscope in order to select a specimen having a grain free of porosity and inclusions providing reproducible measurements. The orientation of the cracks (stripes) was determined to ±2° with light optical microscope under brightfield illumination at 400× and marked as the reference direction.

The optical properties of the as-polished substrate were also studied. Ellipsometric measurements were performed on the same etched grain that was previously identified and selected. After measurements in the etched condition, grain boundaries were marked; the specimen surface was slightly polished, rinsed in anhydrous ethyl alcohol and finally dried with a blast of air.

The anisotropy of reflection observed under diffuse light was characterized with a null ellipsometer, sketched in Fig. 2a. The reflection intensity of unpolarized light at oblique incidence was measured after polishing and after etching. The reflection intensity for the polarization parallel to the plane of incidence (p) and perpendicular to it (s) were measured for incident angles (φ) of 55°, 60°, 65° and 70°. The wavelength (λ) of the beam was varied from 400 nm to 700 nm by steps of 10 nm. The orientation of stripes (θ) was varied over 360° at 10° intervals in the clockwise direction. The diameter of the incident beam was about 3 mm so it could be directed entirely on the etched grain even at 70° of incidence. The reflection intensity of unpolarized light (r) was determined by using the following relationship [28]:

$$r = \sqrt{\frac{1}{2}r_p^2 + \frac{1}{2}r_s^2}, \tag{1}$$

where (r_p) and (r_s) are the reflection intensity of the parallel and the perpendicular polarization measured by the ellipsometer, respectively. In order to estimate the reflection intensity detected by the eye for a particular angular orientation of the surface (r_θ), the reflection of unpolarized light was normalized over the 400–700 nm wavelength range taking into account the spectral sensitivity of the eye shown in Fig. 3 [29]. The following relationship was used:

$$r_\theta = \frac{\sum_\lambda r_{\lambda,\theta} s_\lambda}{\sum_\lambda s_\lambda}, \quad \lambda = 400, 410, 420, \ldots 700 \text{ nm} \tag{2}$$

where λ is the wavelength of the incident beam, $r_{\lambda,\theta}$ is the reflection intensity of unpolarized light at a given wavelength (λ) and for a given angular orientation of the surface (θ) and s_λ is the relative spectral sensitivity of the eye at a given wavelength.

A photo-ellipsometer developed by Bader et al. [30], and sketched in Fig. 2b, was used to evaluate

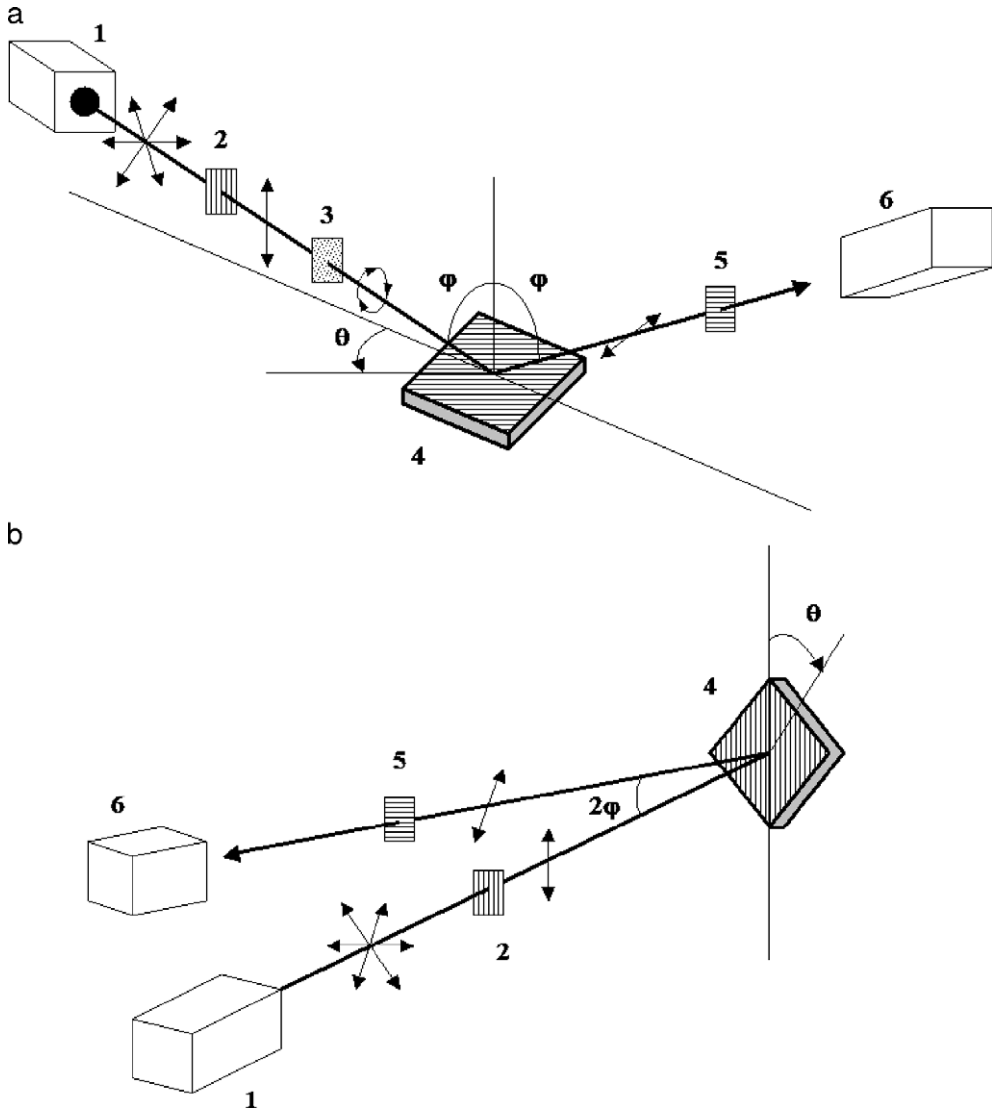

Fig. 2. Schematic view of the experimental set-up used to determine (a) the reflection intensity of unpolarized light at oblique incidence and (b) the phase shift between p and s polarizations at near-normal incidence. 1, light input system; 2, polarizer; 3, compensator; 4, etched specimen; 5, analyzer; 6, detector.

the phase shift upon reflection at near normal incidence after polishing and after etching. The phase shift and the reflection for both (p) and (s) polarizations were measured at an angle of incidence (φ) of 10°. The wavelength of the incident light was varied from 400 nm to 700 nm at 5 nm intervals and the orientation of the surface (θ) was varied over 180° at 10° intervals in the clockwise direction. The specimen was carefully placed in order to align the entire beam over the same grain that was selected for the measurements with the null ellipsometer. In order to obtain the phase shift after reflection as-perceived by the eye at a given surface angular orientation (δ_θ), the phase shift measured by the photo-ellipsometer was normalized over the 400–700 nm wavelength range taking into

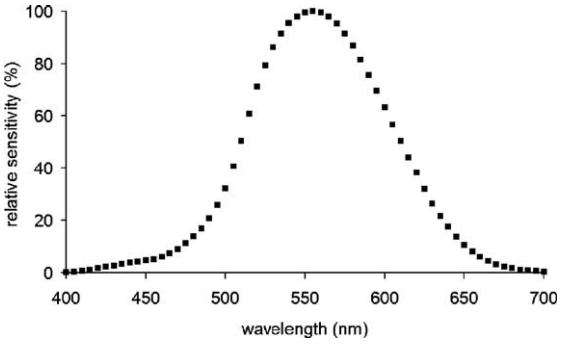

Fig. 3. Spectral sensitivity of the eye over the 400–700 nm range. The sensitivity is highest at 550–560 nm [29].

account the spectral sensitivity of the eye and the reflectivity of the surface:

$$\delta_\theta = \frac{\sum_\lambda \delta_{\lambda,\theta} r_{\lambda,\theta} s_\lambda}{\sum_\lambda r_{\lambda,\theta} s_\lambda}, \quad \lambda = 400, 405, 410, \ldots 700 \text{ nm} \quad (3)$$

where $\delta_{\lambda,\theta}$ is the phase shift between the parallel and the perpendicular polarization measured by the photo-ellipsometer at a given wavelength and for a given angular orientation of the surface.

The etched specimen was examined using light optical microscope with polarized light; the polarizer and the analyzer being perpendicular to each other. A first-order (550 nm) retardation plate was used to determine the fast axis, the slow axis, and the optical sign of birefringence of the etched surface.

4. Results and discussion

4.1. Film texture analysis

Fig. 4 shows SEM micrographs of the etched surface of two different grains in an AZ91D specimen for the three above-described rinsing solutions. Fig. 4a, c and e show a film having preferentially aligned cracks formed at the surface of one grain (the grain being slightly more polished from 4a to 4e). The orientation of cracks is the same and it depends on the crystallographic orientation of underlying grain. For the other grain, the micrographs of Fig. 4b, d and f show no preferential alignment.

The film texture is greatly influenced by the rinsing solution. Alcohol promotes the formation of cracks

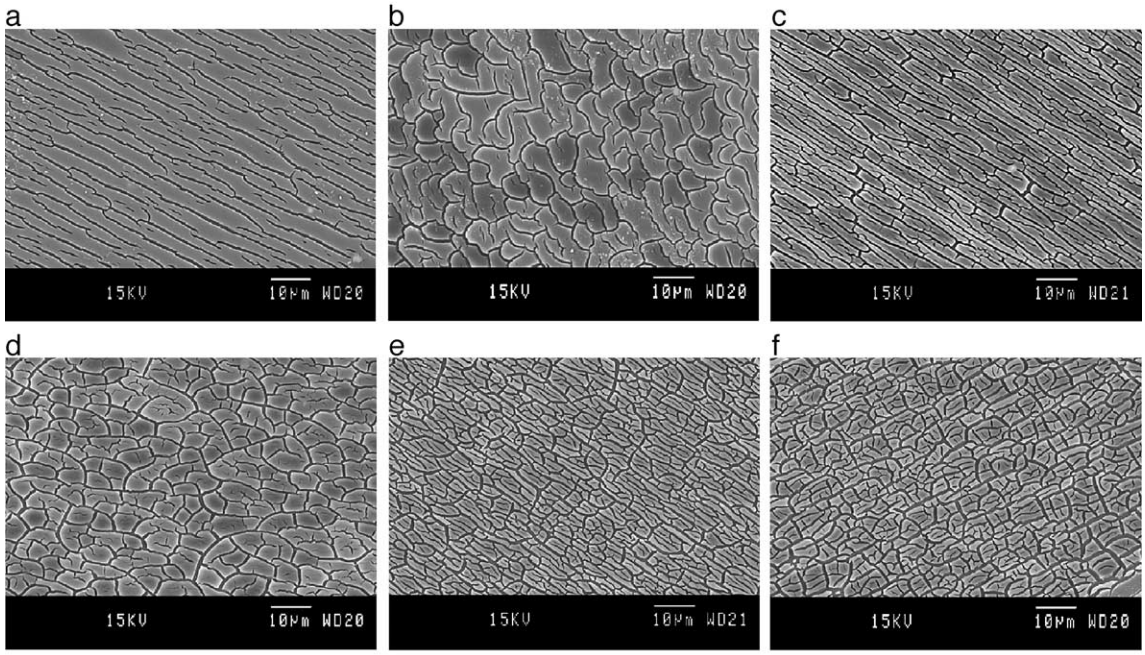

Fig. 4. SEM micrographs of the etch surface in a zone where cracks are (a, c, e) preferentially aligned and (b, d, f) unaligned. Drying media: (a, b) alcohol; (c, d) 90% alcohol–10% glycol; (e, f) water.

Table 3
Effect of the rinsing solution on the contrast between grains

Rinsing solution	Contrast between grains	
	Polarized light	Diffuse light
Ethyl alcohol	Excellent	Nil
Distilled water	Poor	Good
90% Alcohol 10% Ethylene glycol	Good	Excellent

with a regular spacing, leaving wide and essentially uncracked surfaces (Fig. 4a and b). The rinsing solution containing ethylene glycol produced shorter but more severe cracking, transversal cracking being also more frequent (Fig. 4c and d). Rinsing with water produced a film with cracks that are even more densely distributed, but with a less definite orientation (Fig. 4e and f). The film peeled off in some areas of specimens rinsed in water.

The aforementioned observations could be explained by different quantity of water extracted from the surface layer prior to drying, which depends on the rinsing solution. Compared with water, the strong hygroscopic power of ethyl alcohol promotes a partial dehydration of the film prior to drying leaving a drier film and producing a crackled film showing less cracks (Fig. 4a and e). The hygroscopicity of the solution containing glycol (Fig. 4c and e) stands between that of water and ethyl alcohol. Also its cracking behavior is intermediate between these two.

The optical behavior of the three film morphologies under diffuse light and under polarized light is summarized in Table 3. The best contrast between grains under cross-polarized light was obtained with alcohol while the solution containing ethylene glycol was best suited for observation under diffuse light.

4.2. Anisotropy analysis

4.2.1. Reflection of unpolarized light at oblique incidence

Fig. 5 shows the reflection intensity of unpolarized light as-perceived by the eye over the 400–700 nm wavelength range as a function of the surface orien-

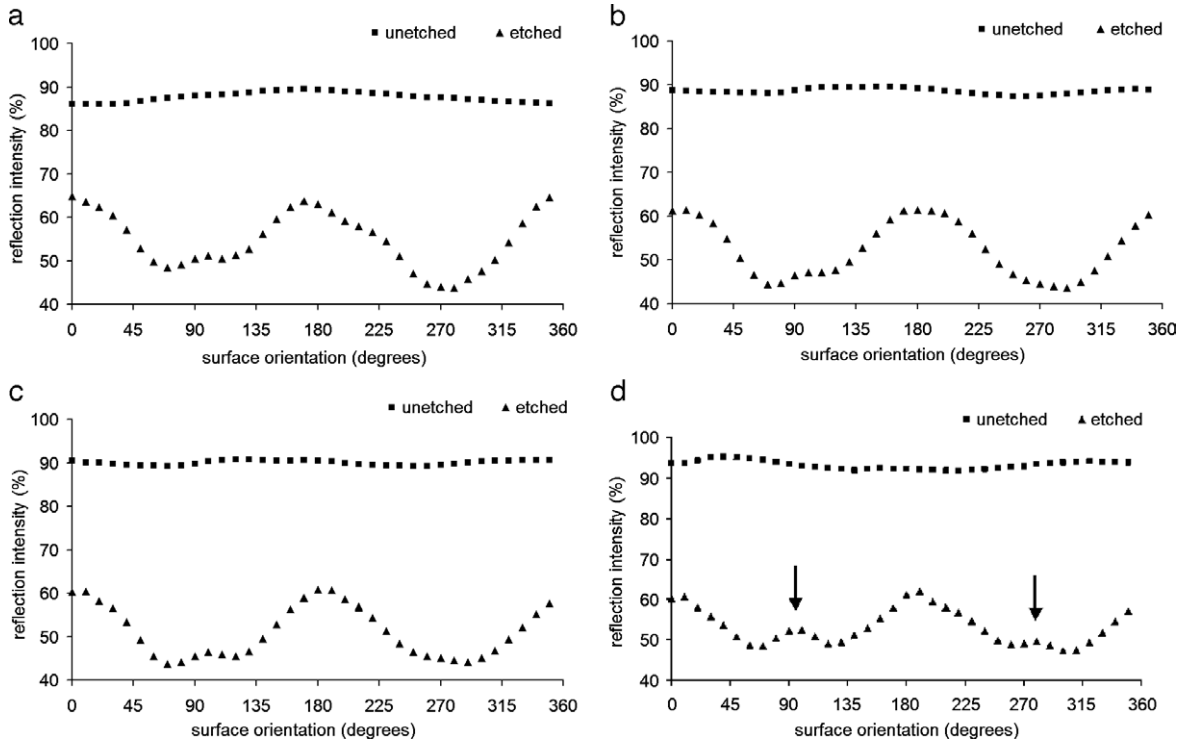

Fig. 5. Reflection intensity as a function of the surface orientation at an incident angle of (a) 55°, (b) 60°, (c) 65° and (d) 70° after polishing and after etching.

tation for incident angles varying between 55° and 70°. For each plot, the surface orientation corresponding to θ=0°, 180°, 360° refers to the incident beam travelling parallel to the stripes in the crackled film.

The reflection intensity of the unetched surface does not vary significantly with the angular orientation of the surface of specimen (Fig. 5). However, the reflectivity of the unetched specimen increases slightly with increasing angle of incidence. It was lower after etching, suggesting a more diffuse reflection due to surface relief and a low reflectivity of the film. The reflectivity of the etched surface was highest when light travelled parallel to the cracks (approx. 0° and 180°) and lowest when it travelled perpendicular to them (approx. 90° and 270°). As seen in Fig. 5a, the reflected intensity varies from 45% to 65%, which corresponds to a variation of about 20% of reflected intensity. As the incident angle increases from 55° to 70° the anisotropy of reflection decreases slightly. In addition, observations of the etched surface of grains at normal incidence with light optical microscope (bright field illumination) revealed that the reflection is isotropic, no contrast being observed. Consequently, there is a maximum of anisotropy near or below 55° but it could not be assessed with the ellipsometer used.

For the highest angle of incidence (70°), secondary maxima of reflection are visible for beams travelling perpendicular to the cracks (see arrows in Fig. 5d). Comparison of Fig. 6a and b shows that the intensity of these secondary maxima also depends on wavelength: they increase as the wavelength of light increases, but they do not depend on the polarization of light (p and s). The reflection anisotropy at oblique incidence can be explained by the morphology of the surface film. An incident beam travelling parallel to the stripes is reflected at the surface of the film and at the surface of the substrate (Fig. 7a). An incident beam travelling perpendicular to the cracks is "trapped" (Fig. 7b) or partially transmitted (Fig. 7c) depending on the angle of incidence and the wavelength of light.

4.2.2. Phase shift and birefringence at near normal incidence

Fig. 8 shows the phase shift of the surface as a function of the crack orientation after polishing and after etching. For each plot, θ=0° and 180° refer to the same orientation, which corresponds to incident light being polarized parallel to the cracks and the plane of incidence.

Fig. 8a shows that the mechanically polished surface is isotropic: the phase shift of the unetched specimen is about 180° and it does not depend on the angular orientation of the surface. Such a phase shift is expected since an incident wave always undergoes a phase inversion after being reflected at normal incidence by a solid having a higher index of refraction than air. Thus, magnesium does not exhibit anisotropy after mechanical polishing despite its closed-packed hexagonal crystalline structure. A similar behavior has been noted by Ernst and Laves [31] and attributed to the disturbed surface caused by mechanical polishing [32].

After etching, the phase shift varies with the angular orientation of the surface (see Fig. 8b). The

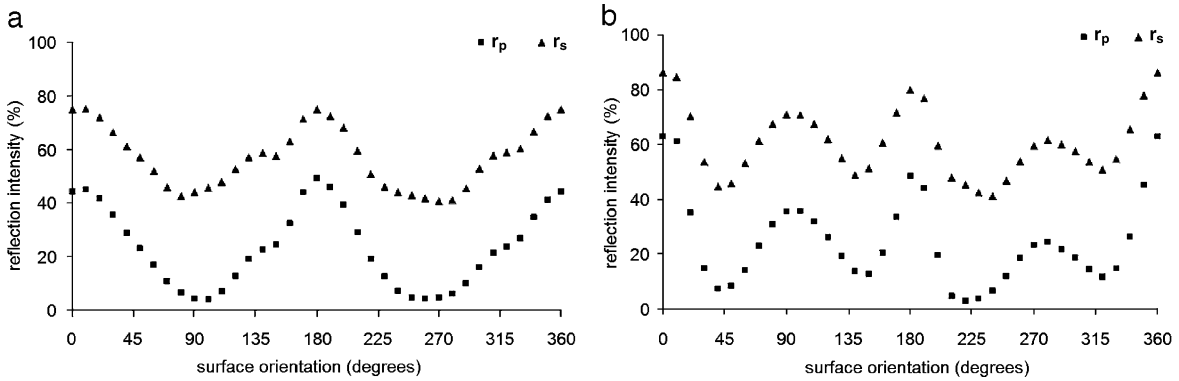

Fig. 6. Reflection intensity of the parallel and the perpendicular polarization as a function of surface orientation after etching at an incident angle of 60° for a wavelength of (a) 400 nm and (b) 700 nm.

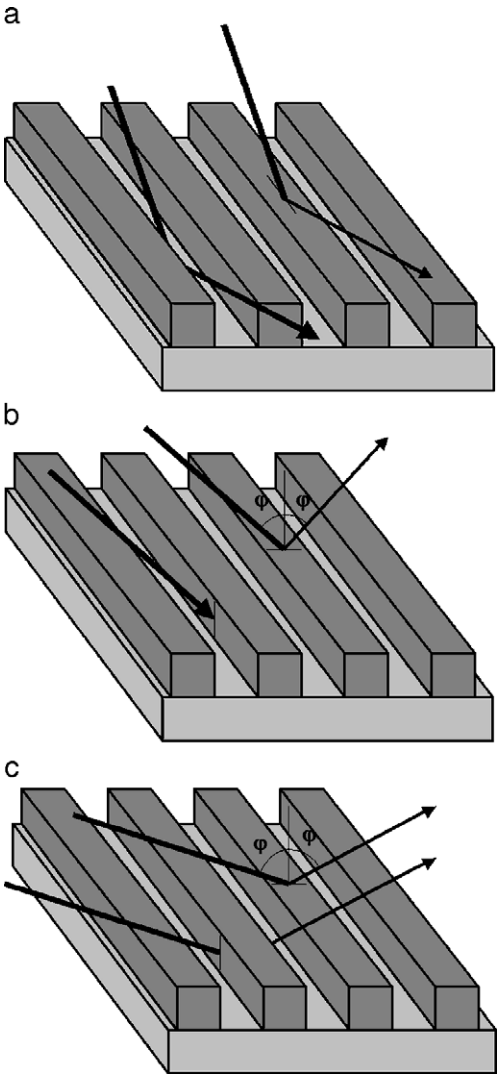

Fig. 7. Reflection of light at oblique incidence on the etched surface. (a) For a beam travelling parallel to the cracks light is reflected at the surface of the film and at the surface of the metal. For a beam travelling perpendicular to the cracks, light is also reflected at the surface of the film but it can be (b) trapped or (c) partially transmitted depending on the angle of incidence and the wavelength of light.

phase shift caused by the surface film itself is greatest at orientations of 45° and 135° because it differs from the phase inversion caused by the reflection at these angles the most. For these orientations, the (p) and (s) wave fronts of the incident beam vibrate parallel and perpendicular to the cracks. Consequently, the fast and the slow axis of the surface film correspond to an orientation perpendicular and parallel to the cracks. However, the fast and slow axis could not be distinguished with the photo-ellipsometer because phase shifts of (180°+x) and (180°−x) are equivalent.

The birefringence (Δn) of the crackled surface film can be calculated from the phase shift measurements using the following relationship [33]:

$$\Delta n = |n_p - n_s| = \frac{(\delta_{\max} - \delta_{\min})\lambda}{4\pi d}, \quad (4)$$

where $\delta_{\max}$=179° (3.12 rad) and $\delta_{\min}$=167° (2.91 rad) are the maximum and the minimum phase shift obtained from Eq. (3) and d=500 nm [1] is the average thickness of the surface layer. Thus, the average birefringence of the etched surface perceived by the eye over the 400–700 nm wavelength range is about 0.018.

4.2.3. Anisotropy under cross-polarized light

Under cross-polarized light with the retardation plate in place, the grain appears yellow when the cracks are oriented Northeast–Southwest (↙↗) while it appears blue if they are oriented Northwest–Southeast (↖↘). According to the Michel-Levy interference chart [34], the aforementioned colors refer to a retardation of about 450 nm and 650 nm, respectively. Consequently, the etched surface produces a maximum retardation of 100 nm since the compensation plate gives a retardation of 550 nm. The slow axis of the retardation plate being oriented Northeast–Southwest (↙↗), it is assumed that the fast axis (low index) is parallel to the cracks since the retardation is added when the cracks are oriented perpendicularly. Therefore, the slow axis (high index) is parallel to the cracks.

The optical axis (isotropic axis) of the surface is perpendicular to the cracks and the surface because the film anisotropy is in the axis of propagation and its properties are equivalent for both (p) and (s) polarizations. This implies that birefringence is negative (n_e<n_o) since the optical axis is the slow axis (Fig. 9). The birefringence (Δn) of the etched surface can be calculated with the following relationship:

$$\Delta n = \frac{\Gamma_{\text{film}}}{2d}, \quad (5)$$

where the maximum retardation (or path difference) caused by the etched specimen (Γ_{film}) is 100 nm. This calculation gives a birefringence of 0.10, which is

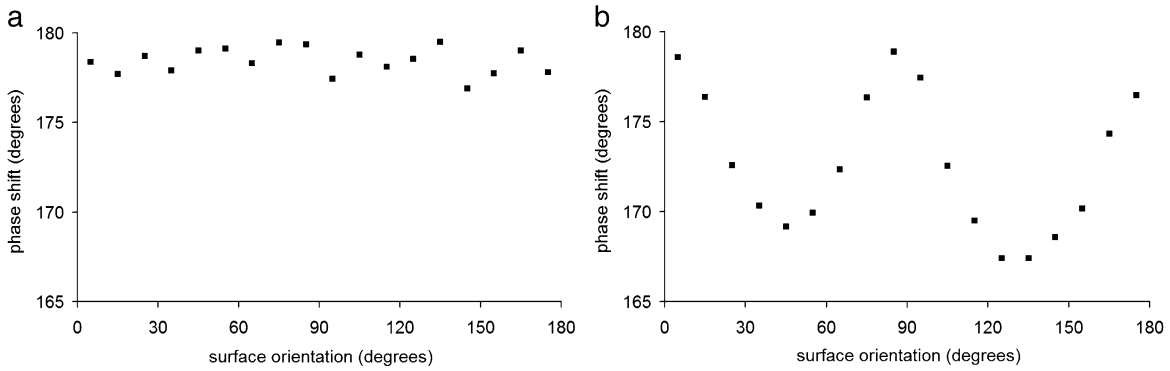

Fig. 8. Phase shift between the p and s polarizations after reflection from the surface (a) after polishing and (b) after etching at an angle of incidence of 10°.

more than five times higher than the birefringence calculated from the ellipsometric measurements. These discrepancies will be discussed in the next section.

4.2.4. Explanation of the optical contrast

The crackled surface film is about 500 nm thick [1], which is comparable to the wavelength of the incident light. However, they are 8.5 μm apart in average as shown in Fig. 10. Thus, the size of the periodic structure is more than an order of magnitude larger than the wavelength of the incident light. Consequently, birefringence must occur only near the cracks and the film is optically isotropic elsewhere.

The disparity of birefringence obtained with the ellipsometer and with the polarizing microscope can be explained by the wavelength (λ) and retardation (Γ) dependence of light passing through the analyzer. If the polarizer and the analyzer polarization axis are crossed and the light is normally incident to the surface, the intensity of light passing through the analyzer (i) is given as follows [33]:

$$i = \frac{i_0}{2}[1 - \cos(\delta)] \tag{6}$$

where i_0 is the intensity of light emerging from the polarizer and δ is the phase shift:

$$\delta = \frac{2\pi\Gamma}{\lambda} \tag{7}$$

Then, if (i) is normalized over the 400–700 nm wavelength range taking into account the spectral

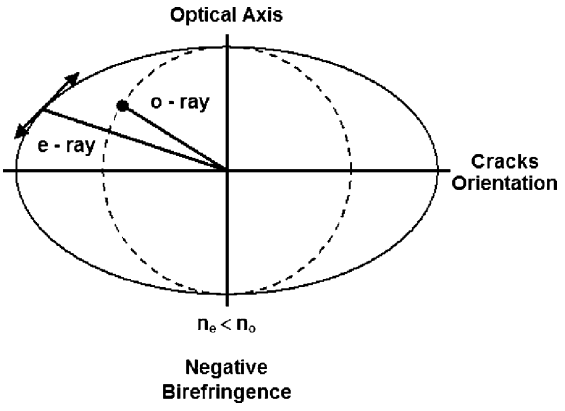

Fig. 9. The etched surface acts as a uniaxial crystal exhibiting positive birefringence with its optical axis being perpendicular to the cracks.

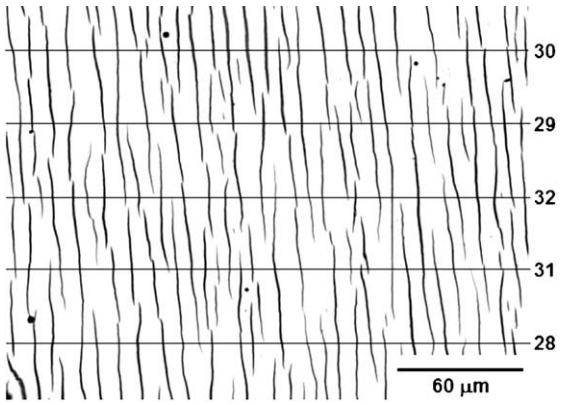

Fig. 10. Aspect of the crackled film under brightfield illumination. The average distance between cracks was evaluated with the linear intercept method. Five fields of 255 μm in length were selected randomly for this purpose. The number of intercept is indicated on the right.

sensitivity of the eye (s_λ), the intensity of light transmitted through the analyzer which is detected by the eye (I) is obtained:

$$I = \frac{\sum_{\lambda} i s_\lambda}{\sum_{\lambda} s_\lambda} \qquad \lambda = 400, 405, 410, \ldots 700 \text{ nm} \qquad (8)$$

Therefore, if a 550 nm retardation plate is inserted in the optical path of the polarizing microscope, the proportion of light transmitted through the analyzer and detected by the eye, as calculated with Eqs. (6) and (7) is 6%, which is very low. However, it is 34% and 29% for a retardation of 450 nm and 650 nm, respectively (retardation observed when the surface exhibits maximum and minimum birefringence—Section 4.2.3). Thus, the relative intensity of light transmitted through the analyzer as-detected by the eye is about five times higher when the grains appear yellow or blue. Accordingly, the area where the birefringence occurs (*near cracks*) outshines the area where the film is isotropic (*elsewhere*). Moreover, this also explains why the grains are brighter if they are yellow (Γ=450 nm) and blue (Γ=650 nm).

It is concluded that the ellipsometric measurements give the mean birefringence of the film while the polarizing microscope measurements provide the birefringence mostly where it occurs, that is near the cracks. Accordingly, the birefringence of the crackled surface layer is heterogeneous and the polarizing microscope is not appropriate to determine the optical properties of such a film.

5. Conclusions

From the above experiments several conclusions are drawn. The crackling pattern of the film formed by etching depends on the rinsing and drying step. Rinsing the specimen with anhydrous ethyl alcohol is best for microscopic observations while the use of a 90% alcohol–10% glycol solution is recommended for macroscopic observations.

After mechanical polishing, the crystal of AZ91D is optically isotropic. The reflection intensity of unpolarized light at oblique incidence and the phase shift at near-normal incidence do not depend on the angular surface orientation of the crystal. These measurements are confirmed by the absence of visual contrast under polarized light.

After etching, the grains are optically anisotropic. The reflection intensity of unpolarized light at oblique incidence depends on the orientation of the surface but it is only slightly influenced by the incident angle in the 55–70° range. Furthermore, the phase shift at near-normal incidence varies as a function of the surface orientation.

According to ellipsometric measurements, the birefringence of the etched surface is 0.018 while it is about 0.10 according to measurements with the polarizing microscope. This difference is explained by the fact that birefringence occurs only near the cracks, the surface film being isotropic elsewhere. The etched grains act as a negative uniaxial crystal having its optical axis perpendicular to the orientation of the cracks.

Acknowledgements

This research was financially supported by grants from National Science and Engineering Research Council Canada (NSERC), FCAR and CERPIC Center. The professional assistance of M. Larouche for metallography, A. Ferland for SEM micrographs and G. Paul-Hus for ellipsometric measurements was greatly appreciated. The authors also acknowledge the contribution of Hydro Magnesium (Bécancour, Canada) for kindly supplying the AZ91D alloy used in this study.

References

[1] Maltais A, Fiset M, Laroche G, Turgeon S, Dubé D. Improvement in metallography of As-Cast AZ91 alloy. Mater Charact 2004;52:103–19.

[2] Maltais A, Fiset M, Dubé D. Influence of vibrations on solidification and moulding of magnesium alloys. Proceedings of the international symposium on enabling technologies for light metals and composite materials and their end-products (Light Metals 2002). Montréal: Canadian Institute of Mining and Metallurgy; 2002 (Aug 11–14). p. 115–26.

[3] Maltais A, Fiset M, Dubé D. Grain refinement of magnesium alloy AZ91D cast in permanent mold using mechanical vibrations. Mat Sci Forum 2003;426–432:527–32.

[4] Maltais A, Dubé D, Fiset M. Metallography of Mg–Al alloys: influence of aluminum and other alloying elements on color etching, [in preparation].

[5] Yano E, Tamura Y, Motegi T, Sato E. Effect of carbon powder on grain refinement of an AZ91E magnesium alloy. Mater Trans 2003;44(1):107–10.
[6] Karlsen DO, Oymo D, Westengen H, Pinfold PMD, Stromhaug SI. Development of grain refiner for Al-containing Mg-Alloys. Proceedings international symposium: light metals processing and applications. Quebec (Canada): Canadian Institute of Mining; 1993. p. 397–408.
[7] Nishoto N, Kawahara H, Shimizu Y, Iwahori H. Grain refinement of magnesium casting alloys by boron addition. In: Kainer KU, editor. Magnesium Alloys and their Applications; 2000. p. 59–64.
[8] Mahoney CH, Tarr AL, Legrand PE. A study of factors influencing grain size in magnesium alloys and a carbon inoculation method for grain refinement. Trans Am Inst Min Metall Pet Eng Inc 1945;1892:1–20.
[9] Luo A. Processing, microstructure, and mechanical behavior of cast magnesium metal matrix composites. Metall Mater Trans, A Phys Metall Mater Sci 1995;26A(9):2445–55.
[10] Tiner N. Superheating of magnesium alloys. Trans Am Inst Min Metall Eng 1945;1935:1–19.
[11] Tamura Y, Haitani T, Yano E, Motegi T, Kono N, Sato E. Grain refinement of high-purity Mg–Al alloy ingots and influences of minor amounts of iron and manganese on cast grain size. Mater Trans 2002;43(11):2784–8.
[12] Cao P, Qian M, StJohn DH. Effect of iron on grain refinement of high purity Mg–Al alloys. Scr Mater 2004;51:125–9.
[13] Tamura Y, Motegi T, Kono N, Sato E. Effect of minor elements on grain size of Mg–9%Al alloy. Mater Sci Forum 2000;350–351:199–204.
[14] Lee YC, Dahle AK, StJohn DH. The role of solute in grain refinement of magnesium. Metall Mater Trans, A Phys Metall Mater Sci 2000;31A(11):2895–906.
[15] Schaffer PL, Lee YC, Dahle AK. The effect of aluminum content and grain refinement on porosity formation in Mg–Al alloys. Magnesium technology 2001; TMS annual meeting. New Orleans, LA, February 11–15; 2001. p. 87–94.
[16] Fox FA, Lardner E. An exploration of the problem of superheating in magnesium-based alloys. J Inst Met 1945; 71:1–22.
[17] Thomson J, Sadayappan K, Liu P, Sahoo M. The effect of C_2Cl_6 on the mechanical properties and microstructure of gravity permanent mold cast AZ91E. Proceedings of the 108th metalcasting congress. Rosemont, IL, June 12–15; 2004.
[18] Iron and steel institute. Metallography 1963. The Iron and Steel Institute; 1964. p. 80.
[19] Metals handbook, Ninth edition. Metallography and microstructures, vol. 9. Metals Park (OH): American Society for Metals; 1989. p. 135–54.
[20] Vander Voort GF. Tint etching. Met Prog 1985;127(3):31–41.
[21] Jones O. Reflexion of plane polarized light by etched metals. Philos Mag, Suppl 6 1924 (July);48(283):207–16.
[22] Charles SB, Levenson LH. Determination of orientation by Etch Pits. Trans Am Inst Min Metall Eng 1940;137:76–84.
[23] George PF. Some special metallographic techniques for magnesium alloys. Trans ASM 1947;38:686–708.
[24] Lalanne P, Lemercier-Lalanne D. Depth dependence of the effective properties of subwavelength gratings. J Opt Soc Am A 1997;14:450–8.
[25] Rytov SM. Electromagnetic properties of a finely stratified medium. Sov Phys JETP 1956;2:466–75.
[26] Mott BW, Haines HR. Examination of metals under polarized light, II applications. Res: J Sci Appl (Lond) 1951;4(2):63–73.
[27] Metals handbook, Ninth edition. Metallography and microstructures, vol. 9. Metals Park (OH): American Society for Metals; 1989. p. 425–34.
[28] Azzam RMA, Bashara NM. Ellipsometry and Polarized Light. Amsterdam, The Netherlands: Elsevier; 1987. p. 141–7.
[29] Williamson SJ, Cummins HZ. Light and Color in Nature and Art. New York: Wiley; 1983. p. 173.
[30] Bader G, Ashrit PV, Girouard FE, Truong VV. Reflection–transmission photoellipsometry: theory and experiments. Appl Opt 1995;34(10):1684–91.
[31] Ernst T, Laves F. Über die Verformung des Magnesiums und seiner Legierungen. Z Metkd 1949;40(1):1–12.
[32] Wernick S, Pinner R, Sheasby PG. The surface treatment and finishing of aluminium alloys. Metals Park (OH): American Society for Metals; 1987. p. 28.
[33] Enger RC, Case SK. Optical elements with ultrahigh spatial-frequency surface corrugations. Appl Opt 1983;22(20): 3220–8.
[34] Bloss FD. Optical Crystallography. MSA monograph, vol. 5. Washington (DC): Mineralogical Society of America; 1999.